Journal of Ceramic Processing Research. Vol. 25, No. 4, pp. 673~682 (2024)
(Received 22 May 2024, Received in revised form 9 July 2024, Accepted 16 July 2024)
https://doi.org/10.36410/jcpr.2024.25.4.673

J O U R N A L O F
Ceramic Processing Research

Effect of Al_2O_3 content on bonding characteristics of CaO-Al_2O_3-SiO_2-TiO_2-ZnO based glass-ceramic on ceramic substrate

Youna Lim, Seunggu Kang and Kangduk Kim*
Department of Advanced Material Engineering, Kyonggi University, Suwon 16227, Korea

This work studies the use of the CaO-Al_2O_3-SiO_2-TiO_2-ZnO (CASTZ)-based glass-ceramics, as a coating and bonding agent was observed according to the change in Al_2O_3 substitution amount. Heat-treatment at 1000°C is the standard procedure for bonding glass-ceramics with Al_2O_3 ceramics. The properties of the glass-ceramics and coatings are examined using X-ray diffraction, scanning electron microscopy, hardness measurements, and Raman analyses, to confirm the actual bonding morphologies and thermal expansion coefficients. Titanite ($CaTiSiO_5$) and willemite (Zn_2SiO_4) crystal phases are observed depending on the amount of Al_2O_3 substitution, and as the substitution amount increases, anorthite ($CaAlSi_2O_8$) crystal phases appear together. At this time, the microstructure densification and hardness change with variation in the heat-treatment temperature, indicating structural impact on glass, which is confirmed by Raman spectroscopy. A comparative analysis of the coefficients of thermal expansion between the substrate and glass-ceramic, along with actual bonding, reveals an increase in the bonding and wettability at higher Al_2O_3 substitution levels.

Keywords: Glass-ceramics, CTE, Titanite, Hardness, Microstructure

Introduction

Glass and glass-ceramic exhibit excellent compatibility with specific metal substrates, making them suitable for applications such as coating for the corrosion protection of metal alloys or titanium alloys at high temperatures [1]. In addition, interest in glass-ceramic is very high owing to its advantages of being able to completely seal the substrate and insulate it from corrosive media, while ensuring chemical compatibility and control of the coefficient of thermal expansion (CTE) between the substrates [1, 2]. CaO-Al_2O_3-SiO_2-ZnO-based glass-ceramic, exhibits excellent corrosion prevention when applied as a coating on titanium alloys, provided that the crystal growth start temperature is below 850°C. This is because the viscosity of glass decreases when the heat-treatment temperature increases, owing to the relatively low softening point (675°C), increasing the wettability of the glass to the substrate [1]. Glass-ceramics of the CaO-Al_2O_3-SiO_2, ZnO-Al_2O_3-B_2O_3-SiO_2, Nd_2O_3-Al_2O_3-SiO_2, and MgO-Al_2O_3-SiO_2 series have been utilized for bonding alumina ceramics [2]. Zheng et al. [3] have published a study on composite coating of glass-Al_2O_3 material exhibiting an oxidation resistance at 1000°C, specifically for K38G super alloy [1]. However, to utilize glass-ceramics with various compositions of bonding materials for metals and ceramics, further research is required on the effects of the glass structure characteristics on the mechanical properties of glass-ceramics, wettability with substrates, and expansion behaviors under different heat-treatment conditions [1,4].

In the case of silicate glass, it exhibits a characteristic wherein the viscosity changes in response to the structural alteration of the [SiO_4] tetrahedron constituting the glass network, leading to alterations its internal structure and mechanical properties of the glass [5, 6]. These structural changes in the tetrahedral [SiO_4] units of silicate-based glass are influenced by various additives. Metal oxides (MO) of alkali and alkaline-earth metals increase the number of non-bridging oxygen atoms in the Si–O bonds, whereas Al_2O_3 reduces the non-bridging oxygen atoms because of the presence of Al^{3+} ions with ionic radii similar to that of Si^{4+}, thus enhancing the stability of the network between the tetrahedral [SiO_4] units [7, 8].

Raman spectroscopy of glass facilitates the analysis of its structural order, phase transition, and thermodynamic properties, thereby providing information on its structural stability [5]. In the case of silicate-based glass, a broad Raman spectrum in the range of 900-1200 cm^{-1} allows the analysis of changes in the number of bridging oxygens through Q^n units associated with Si-O bending structures. These changes impact the stability of the glass structure and can alter various properties of the glass structures [6, 7, 9].

Therefore, in this study, we investigate the substitution of Al_2O_3 in CaO-Al_2O_3-SiO_2-TiO_2-ZnO-based silicate glass and the effects of various substitution amounts (1-5 mol%) on the glass structure and mechanical properties.

*Corresponding author:
Tel : +82-10-6206-6290
E-mail: solidwaste@kyonggi.ac.kr

In particular, we examine the changes in the bonding and hardness characteristics of glass due to Al_2O_3 addition and analyze the influence of Al_2O_3 on glass structure changes at a heat-treatment temperature of 1000°C, using the Raman spectroscopy results of Q^n variations in the glass network.

Experimental Procedure

$CaCO_3$ (Kojundo Chemicals, Ltd., Japan, 4N), Al_2O_3 (Kojundo chemicals, Ltd., Japan, 4N), SiO_2 (Kojundo Chemicals, Ltd., Japan, 3N), TiO_2 (Kojundo chemicals, Ltd., Japan, 3N), and ZnO (Kojundo Chemicals, Ltd., Japan, 3N) were utilized to manufacture the base glass; their respective blending ratios are presented in Table 1. To mix the raw materials according to the mixing ratio, dry milling was performed for 12 h using zirconia balls (diameter = 5, 10 mm) and a ball mill. Subsequently, the mixture was melted at 1450°C using an alumina crucible, poured into preheated graphite molds at 400°C, and annealed for 1 h. To analyze the characteristics of glass-ceramic, the parent glass was pulverized and sieved to a size of 45 μm or less, and circular (Φ =10 mm) specimens were formed using a hydraulic press under 5 ton/s. The produced specimens were heat-treated in a SiC box furnace (heating rate = 10°C/min) at 1000, 1050, and 1100°C for 5 min each. For observing the bonding characteristics of glass-ceramic, ground and sieved particles below 45 μm were mixed with distilled water (1:1 wt%), coated onto alumina substrates (Al_2O_3 96%) using a syringe, and another substrate was placed on top. The coated substrates were heat-treated at 1000 and 1100°C for 5 min each in a SiC box furnace (heating rate = 10°C/min).

X-ray diffraction (XRD, MiniFlex II, Rigaku Co., Japan) was performed to analyze the crystal phase of the parent glass and glass-ceramic according to changes in the mixing ratio. X-ray photoelectron spectrometer (XPS, K-Alpha, Thermo Fisher Scientific, USA) was performed to analyze the trace elements of the parent glass. For thermal characterization, the parent glass was ground, sieved to a size of less than 45 μm, and measured under conditions of 10°C/min using a differential thermal analyzer (DTA, STA449 F3, Netzsch, Germany). After etching the glass-ceramic in a 3 wt% hydrofluoric acid (HF) solution for 30 s, the surface microstructure was observed using field-emission scanning electron microscopy (FE-SEM, JSM-7610F PLUS, JEOL, Japan). Quantitative elemental analysis of the glass-ceramic surface was performed using energy-dispersive X-ray spectroscopy (EDS, Oxford, JEOL 7610F Plus, UK). The surface hardness of the glass-ceramic was measured under 4.9 N/10 s using a micro-Vickers hardness tester (HM-124, Mitutoyo Co., Japan) applying the ASTM E384-17 standard. The bulk density and water absorption of the glass-ceramic was measured using the Archimedes principle (KS l ISO 18754). To further observe the changes in the glass structure and hardness due to Al_2O_3 substitution, Raman scattering analysis was conducted at room temperature (RT) using a micro-Raman spectrometer (LabRam Armis, Horiba Jobin Yvon, USA). Measurements were performed in the range of 100-1200 cm^{-1} using an Ar-ion laser (514 nm) as the excitation source, with a beam intensity of ~1.0 mW at the surface to prevent specimen damage from heating. The CTE of the glass-ceramic was measured over the range of RT to 800°C at a heating rate of 10 °C/min using a thermomechanical analyzer (TMA Q400, TA Instruments, USA). The final bonding state between the glass-ceramic and alumina substrate was observed using an optical microscope (ECLIPSE LV150N, Nikon, USA).

Table 1. The batch composition of parent glass.

Specimen	Composition (mol%)				
	CaO	Al_2O_3	SiO_2	TiO_2	ZnO
TA0	30	-	40	25	5
TA1		1	39		
TA3		3	37		
TA5		5	35		

Results and Discussion

Figure 1 and Figure 2 show the optical images and XRD analysis results of the parent glass melted at 1450°C for 30 min. All parent glass showed an amorphous peak, a transparent and dark color.

Figure 3 shows the results of XPS analysis of TA5 parent glass, (a) and (b) are the analysis results of Ti and Fe elements, respectively. The peak position and area represent the relative content and binding energy [10]. From the peaks position, the binding energies of $Ti^{3+}2p_{1/2}$ (460.4 eV), $Ti^{4+}2p_{1/2}$ (464.1 eV), $Ti^{4+}2p_{3/2}$ (458.3 eV), $Fe^{2+}2p_{3/2}$ (709.9 eV), and $Fe^{3+}2p_{3/2}$ (714.2 eV) were confirmed [11, 12]. Due to a trace amount of iron impurity, a charge transfer such as $Ti^{3+} + Fe^{3+} \rightarrow Ti^{4+} + Fe^{2+}$ occurred, and a low ratio of Ti^{3+} and a high ratio of Ti^{4+} being observed. It is judged that TA5 appears

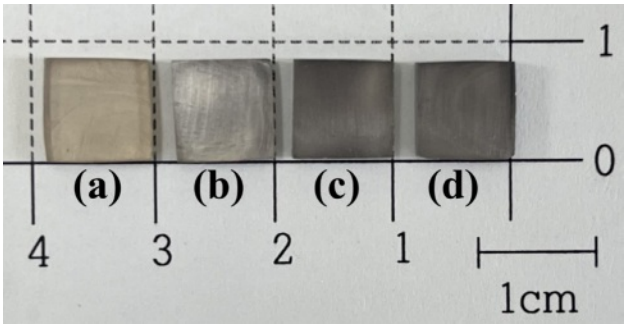

Fig. 1. Optical image of the parent glass; (a) TA0, (b) TA1, (c) TA3, and (d) TA5.

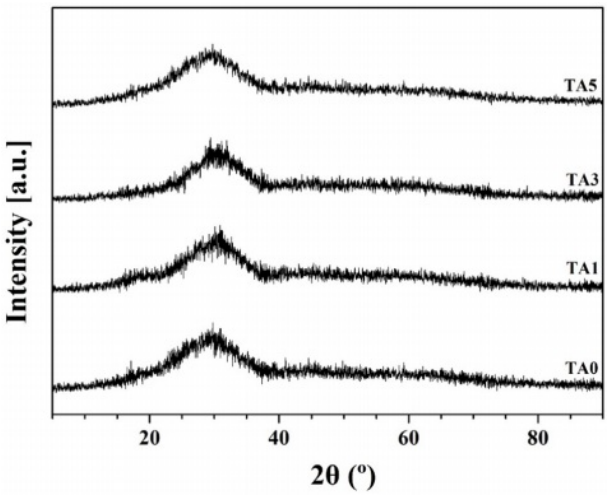

Fig. 2. XRD of the parent glass melted at 1450°C.

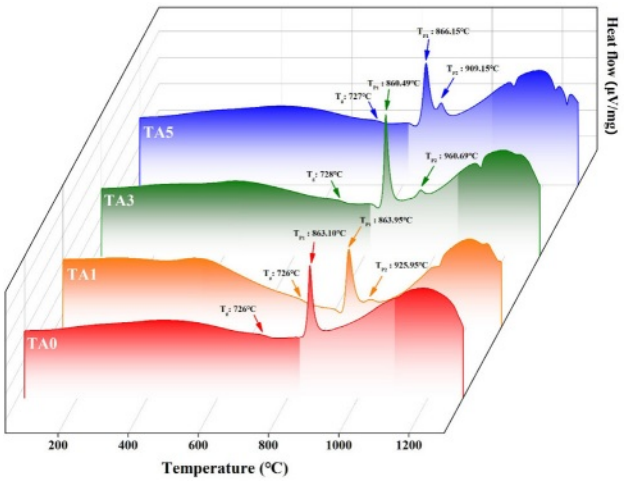

Fig. 4. DTA curves of the parent glass (heating rate = 10°C/min).

dark black due to Ti^{4+} contribution to glass coloration, known as ilmenite coloration [13-15].

Figure 4 shows the results of the DTA measurements of the parent glass, performed under a heating rate of 10°C/min. In the case of the glass transition temperature (T_g), no significant change was observed at TA0 (726°C) regardless of the amount of Al_2O_3 added. For the exothermic peak (T_P), one peak (T_{P1}) was observed at TA0, and a new peak (T_{P2}) emerged with increasing Al_2O_3 substitution. T_{P1} appeared in the range of 860-866°C for each composition. T_{P2} presented a rapid increase from 925.95°C at TA1 to 960.69°C at TA3, and then tended to decrease to 909.15°C at TA5. This increase or decrease in the crystallization temperature was believed to be due to a change in the thermal stability as the bonding strength of the glass structure changed owing to Al_2O_3 substitution [4, 16]. Additionally, the endothermic peaks observed above 1000°C could be attributed to the decomposition of the willemite crystalline phases within the glass [17].

Figure 5 shows the XRD results of the parent glass obtained after 5 min of heat-treatment at temperatures corresponding to the exothermic peaks (T_{P1} and T_{P2}) observed in Figure 4. In the case of TA0, the titanite ($CaTiSiO_5$, ICSD Ref. codes: 98-000-9837) crystalline phase was observed at the crystallization temperature, whereas for TA1, TA3, and TA5 with Al_2O_3 substitution, both titanite and willemite (Zn_2SiO_4, ICSD Ref. codes: 98-001-6172) crystalline phases were observed simultaneously at the crystallization temperatures (T_{P1} and T_{P2}). The simultaneous observation of these crystalline phases suggested that the crystallization of titanite and willemite occurred after heterogeneous nucleation at each exothermic peak [18]. The titanite crystal phase was observed to be the main crystal phase while the willemite crystal phase was relatively low, and could be considered a secondary crystal phase.

Figure 6 shows the XRD analysis results of the parent glass subjected to heat-treatment at temperatures of 1000, 1050, and 1100°C. In the case of TA0, only the titanite crystal phase was observed at the previous crystallization temperature (T_{P1}: 863.10°C); however, as

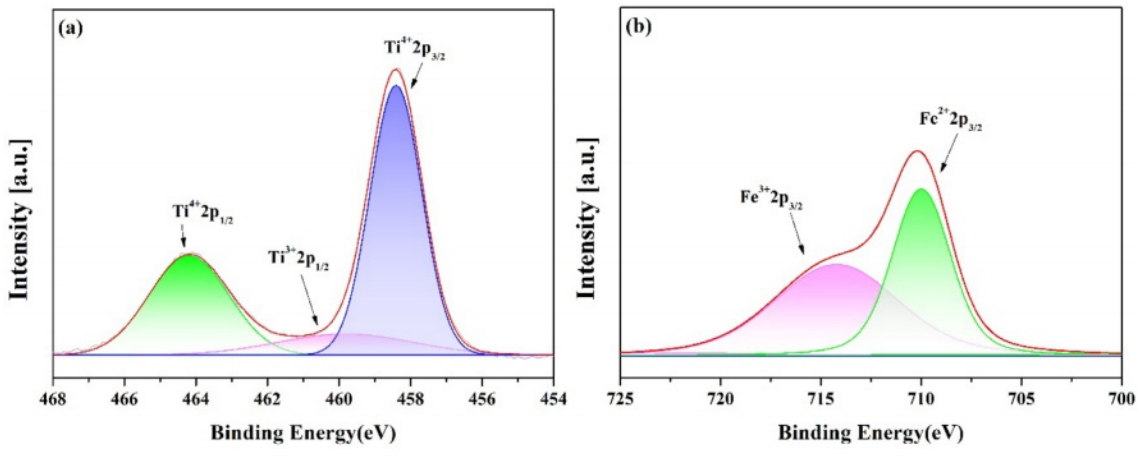

Fig. 3. XPS spectra of Ti and Fe elements in TA5.

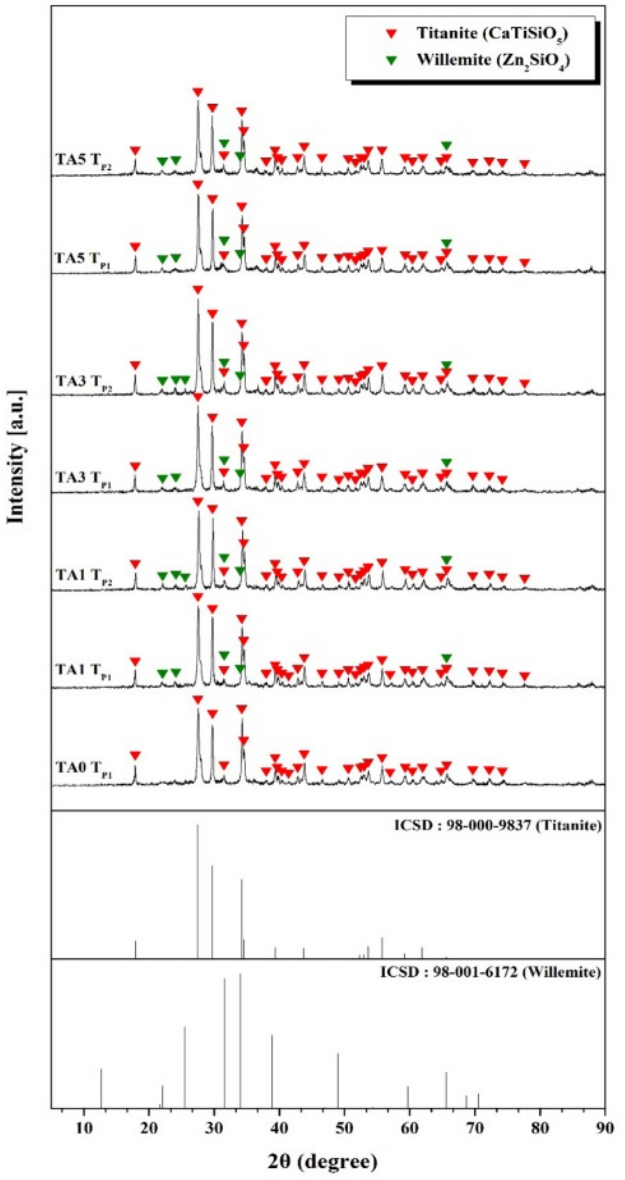

Fig. 5. XRD of parent glass heat-treated at crystallization temperature (T_P).

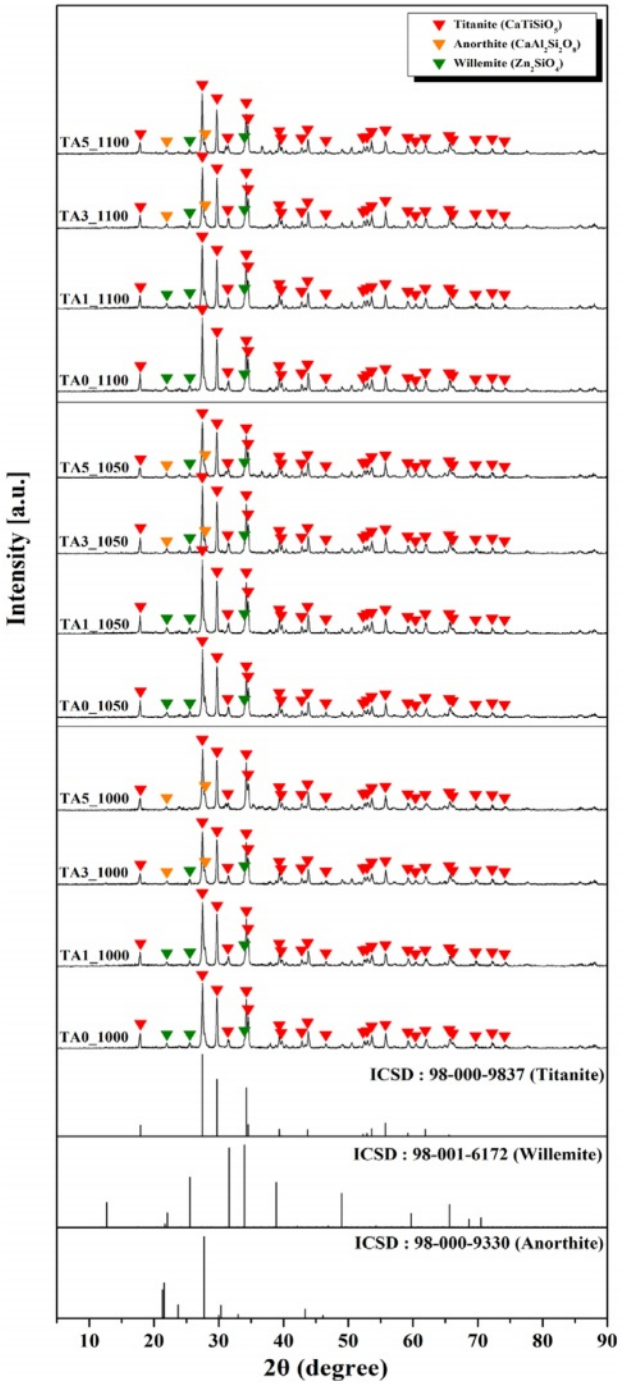

Fig. 6. XRD of parent glass heat-treated at different temperature.

the heat-treatment temperature increased, willemite, a ZnO-related crystal phase, appeared. These characteristics were also confirmed in the results of A. Escardino et.al, who conducted an XRD analysis at different heat-treatment temperatures for CaO-Al_2O_3-SiO_2-ZnO glass-ceramics [19]. Anorthite crystalline phase was formed at a temperature of 900~950°C, and gahnite and willemite crystalline phase were additionally formed as the temperature increased. At temperatures above 1150°C, only the gahnite crystal phase existed. Therefore, it is judged that the titanite and willemite crystalline phase appear together within the heat-treatment temperature range and composition of this study [20]. Therefore, it was believed that the titanite and willemite crystal phases appeared together in the corresponding heat-treatment temperature range and composition. However, with the substitution of 3 mol% Al_2O_3, an anorthite ($CaAl_2Si_2O_8$, ICSD Ref. codes: 98-000-9330) crystalline phase appeared, accompanied by a decrease in the intensity of the willemite crystalline phase.

Figure 7 shows the results of electron microscope surface microstructure observations of specimens heat-treated at 1000, 1050, and 1100°C after etching with HF. In all specimens, dendritic and irregular crystal phases were observed. As the amount of Al_2O_3 substitution increased, the dendritic crystal phase became denser.

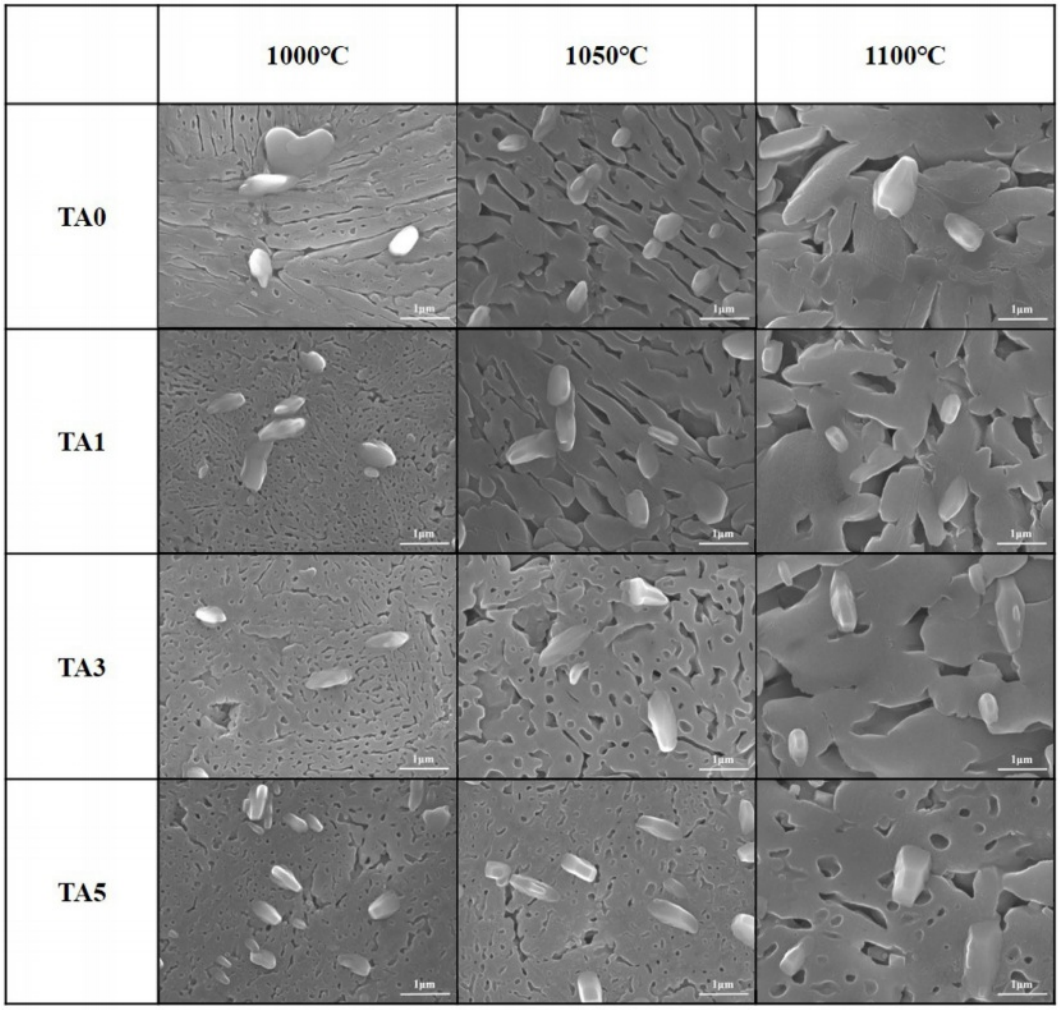

Fig. 7. SEM images of specimens heat-treated at different temperature.

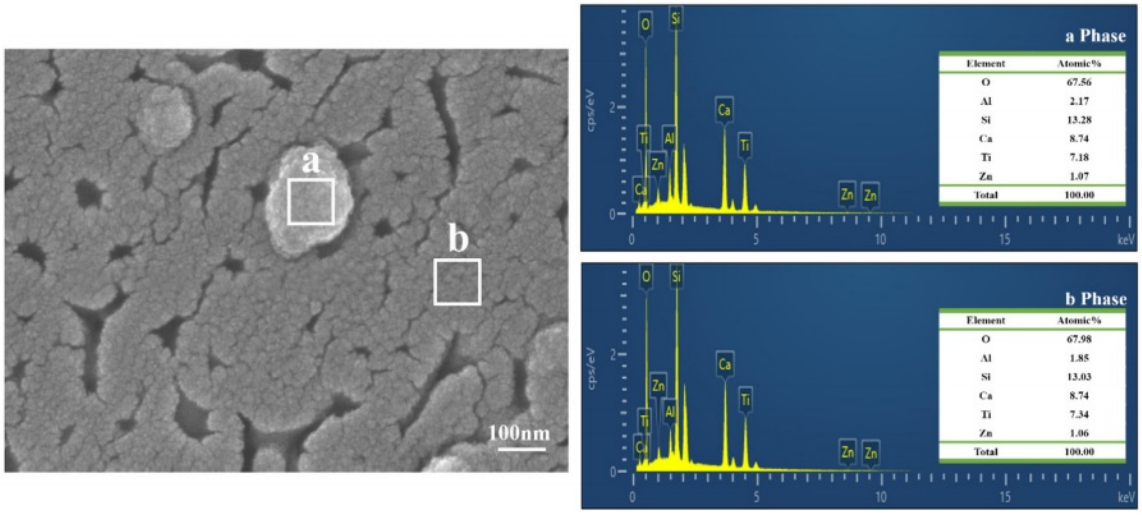

Fig. 8. EDS spectra in areas a and b measured on TA3 heat-treated at 1000°C.

The size of the dendritic crystal phase increased as the heat-treatment temperature increased. This change was believed to be due to the coarsening of the crystal phase with the supply of heat energy as the heat-treatment temperature increased.

Figure 8 shows the EDS analysis results of the TA3

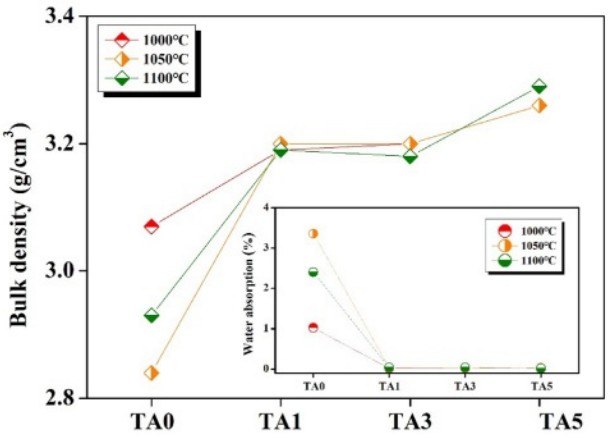

Fig. 9. Bulk density and Water absorption of specimens heat-treated at different temperature.

specimen heat-treated at 1000°C. A subtle quantitative difference can be observed between the Al and Ti in areas a and b; nevertheless, the other elements showed similar values to each other. The microstructural and EDS analyses indicated that area a grew from area b.

Figure 9 shows the bulk density and water absorption of specimens heat-treated at different temperatures. The bulk density of the specimen increased, and the water absorption tended to decrease as the amount of Al_2O_3 substitution increased. It is believed that as the amount of Al_2O_3 substitution increases, Al^{3+} bonds to the silicate structure to form [AlO_4], and the bulk density increases due to densification of the structure through crystal growth [21].

Figure 10 shows the micro-Vickers hardness values of specimens heat-treated at 1000, 1050, and 1100°C. The specimen heat-treated at the lowest temperature of 1000°C exhibited rapid changes in the hardness, according to the change in the Al_2O_3 substitution amount. They exhibited a rapid increase in hardness from 7.48 GPa for TA0 to 8.97 GPa for TA3 with increasing Al_2O_3 substitution,

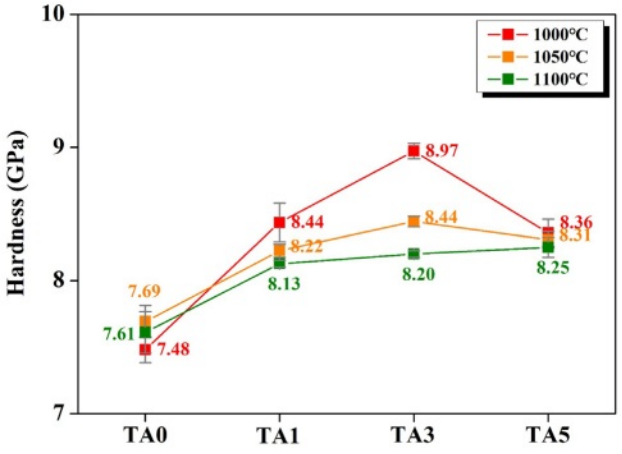

Fig. 10. Micro-Vickers Hardness of specimens heated-treated at different temperature.

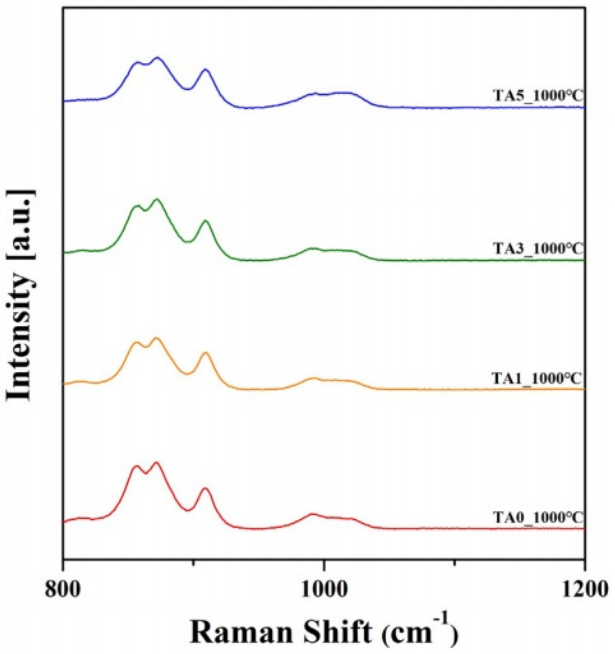

Fig. 11. Raman spectra of specimens heat-treated at 1000°C (800-1200 cm^{-1}).

followed by a decrease to 8.36 GPa for TA5. This change in hardness was attributed to the increased crystallization and densification of the glass owing to the occurrence of T_{P2} induced by Al_2O_3 substitution [20]. Additionally, the tendency of the hardness to decrease with increasing heat-treatment temperature was closely related to the observed increase in crystal size, as shown in Figure 7. The size of the crystal phase is known to directly affect the strength of glass-ceramics with a high crystalline volume fraction [22, 23]. In the case of crystals of a certain size, the interlocking of crystals prevents crack propagation within the glass matrix, thereby preventing a decrease in the strength [22, 23]. However, for larger crystals, crack propagation is facilitated, leading to a decrease in hardness [22, 23].

Figure 11 shows the Raman spectrum results of specimens heat-treated at 1000°C. The Raman peak intensity was observed through XRD and temperature dependent hardness changes through the corresponding Raman spectrum analysis as a function of not only the frequency but also bond polarizability. The spectrum observed at approximately 800-1200 cm^{-1} was confirmed to be the most important range for the silicate system, showing SiO_4 tetrahedral structural bonding and typical titanite peaks [5, 24-27].

Figure 12 shows the deconvolution of the Raman spectrum presented in Figure 11. The degree of polymerization of the SiO_4 tetrahedral structural bonds in glass is usually estimated by the relative content of Q^n species (n = 0, 1, 2, and 4), which indicates the number of oxygen atoms bridged in the [SiO_4] units [5, 28]. Each value can be characterized by qualitatively comparing the degree of polymerization of the glass composition

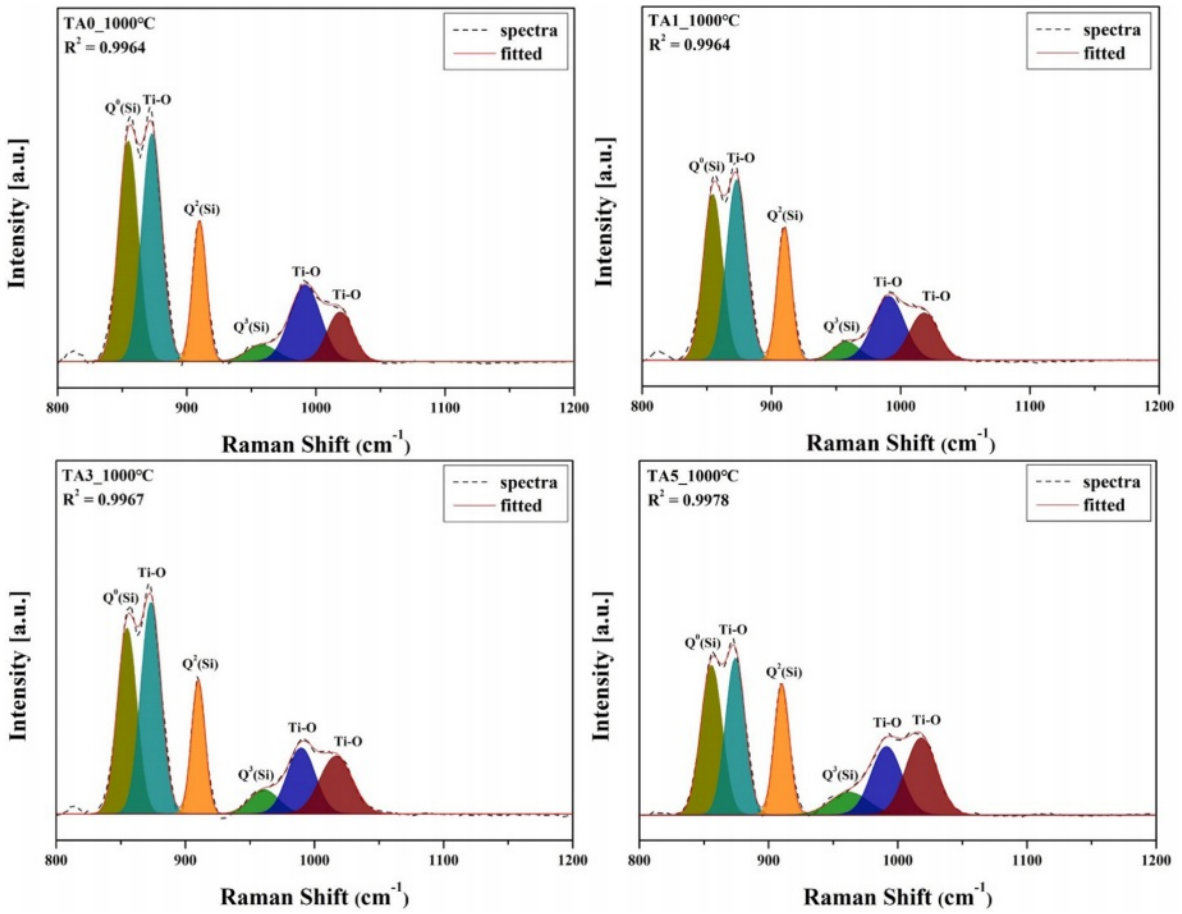

Fig. 12. Deconvolution of Raman spectra of specimens heat-treated at 1000°C (800-1200 cm^{-1}).

using the relative ratio and deconvoluted area of each Q^n unit [29]. Thus, based on specific Q^n units (where n represents the number of bridging oxygen atoms), the band positions could be distinguished. Structurally, NBO/Si varied from 0 to 4, commonly known as Q^4 = three-dimensional network [SiO_2] (1190-1200 cm^{-1}), Q^3 = sheets [Si_2O_5]$^{2-}$ (1050-1100 cm^{-1}), Q^2 = chains [Si_2O_6]$^{4-}$ (950-980 cm^{-1}), Q^1 = dimers [Si_2O_7]$^{6-}$ (900-920 cm^{-1}), and Q^0 = monomers [SiO_4]$^{4-}$ (850-880 cm^{-1}) [24]. At this time, Raman bands were observed in the range of Q^0(Si) at 854.6-855.6 cm^{-1}, Q^2(Si) [30, 31] at 960.4-964.6 cm^{-1}, and Q^3(Si) [31] at 960.4-964.6 cm^{-1}. Raman bands typical of titanite crystal phases were observed at 872.9-874.1 cm^{-1}, 990.6-991.6 cm^{-1}, and 1017.9-1020.0 cm^{-1} [26].

Figure 13 and Table 2 show the peak area distribution and area percentage of [SiO_4] Q^n obtained through the deconvolution of the Raman bands confirmed in Figure 12. The area% of Q^2 and Q^3 were named AQ^2 and AQ^3, respectively, and the ratio of AQ^3/AQ^2 was used as an indicator to determine the changes in the distribution of the Q^n species [7]. In the case of Q^0(Si), it clearly decreased from 63.82 to 57.08 %, whereas Q^2 and Q^3 tended to increase. In addition, when changing from TA0, in which Al_2O_3 was not substituted, to TA1,

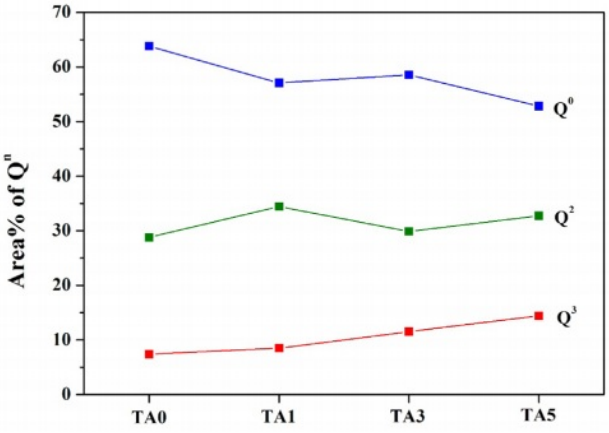

Fig. 13. Peak area of Q^n in specimens heat-treated at 1000°C.

the ratio of AQ^3/AQ^2 decreased and the area ratio exhibited a tendency to increase thereafter. The main cause of the decrease in AQ^3/AQ^2 in the distribution of Q^n was the increase in strain owing to the distortion of the tetrahedral structure. The increase in AQ^3/AQ^2 has been known to increase the stability of the network because of the increase in the Al_2O_3 content replacing SiO_2 [7]. This indicated that Al_2O_3 entered the silicate

Table 2. The peak area distribution and area percentage of $[SiO_4]$ Q^n obtained through the deconvolution of the Raman bands.

	TA0		TA1		TA3		TA5	
Network structure	int area	% area	int area	% area	int area	% area	int area	% area
[1)]Q^0	1.64	63.82	1.21	57.08	1.37	58.55	1.21	52.84
[2)]Q^2	0.74	28.79	0.73	34.43	0.70	29.91	0.75	32.75
[3)]Q^3	0.19	7.39	0.18	8.49	0.27	11.54	0.33	14.41
AQ^3/AQ^2		0.26		0.24		0.39		0.44

[1)]Q^0 ν range (cm^{-1}): 854-856
[2)]Q^2 ν range (cm^{-1}): 910
[3)]Q^3 ν range (cm^{-1}): 963

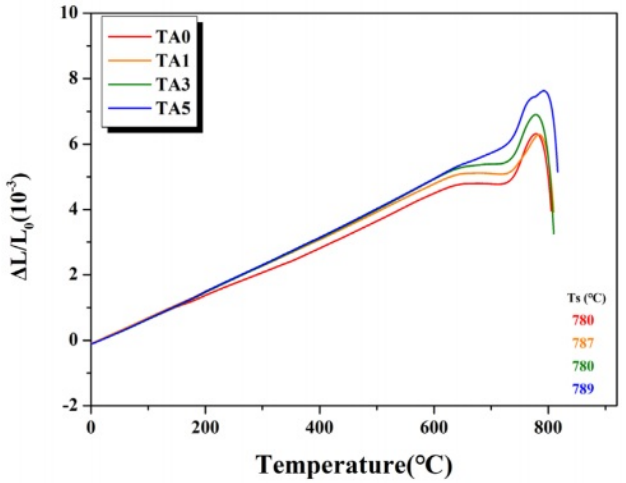

Fig. 14. Thermal expansion curves of specimens.

Table 3. Thermal expansion coefficient of specimens.

	TA0	TA1	TA3	TA5
α × 10^{-6}/°C (30-600°C)	7.7	8.2	8.5	8.5

network in the form of $[AlO_4]$ tetrahedra, increasing the stability of the network, reducing the number of non-bridging oxygen atoms, and providing a denser and more stable structure [7]. Therefore, it could be inferred that the increase in network stability owing to the increase in Al_2O_3 substitution and the highest hardness value observed for TA3 were due to the optimal Al_2O_3 content.

Figure 14 and Table 3 show the thermal expansion curve and CTE value in the range of RT to 600°C. Matching the CTE of the joining components is a

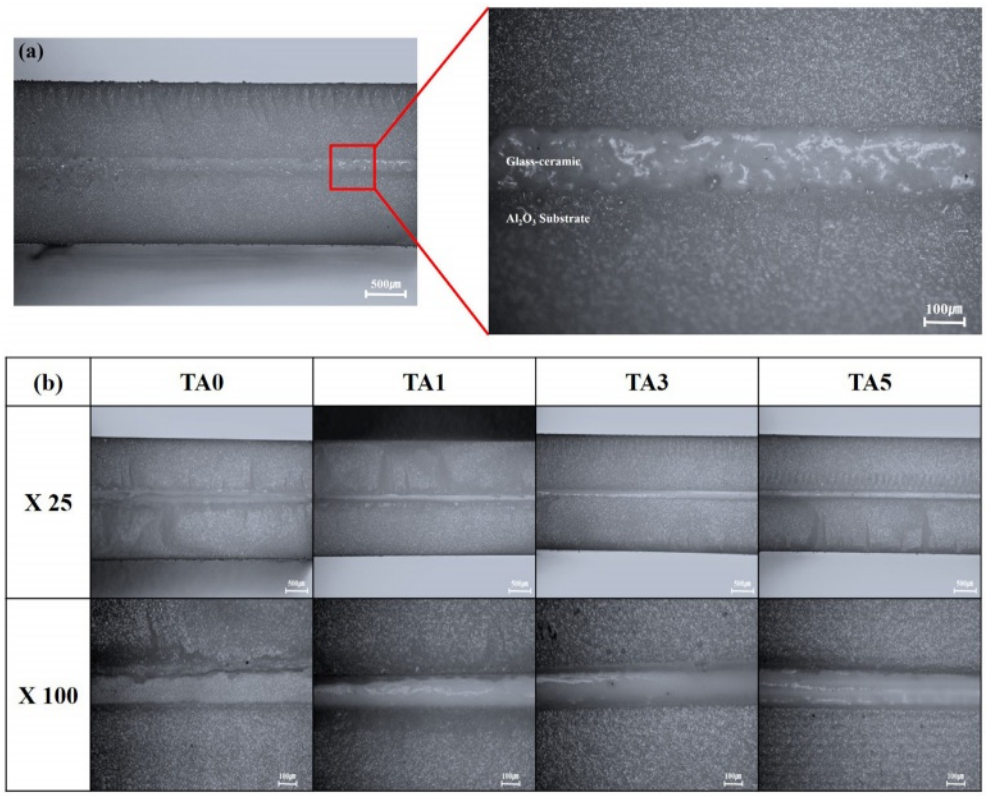

Fig. 15. Optical image of junction; (a) TA5 heat-treated at 1000°C, (b) specimens heat- treated at 1100°C.

primary condition for high-strength bonding in the case of joined coated glass-ceramics [2]. For ceramics mainly used as joining components, the CTE values of Al_2O_3 (7.4×10^{-6}/°C [32]), ZrO_2 (10.5×10^{-6}/°C [33]), and ZTA (8.5×10^{-6}/°C [33, 34]). The glass-ceramic in this study is TA0 (7.693×10^{-6}/°C), TA1 (8.156×10^{-6}/°C), TA3 (8.456×10^{-6}/°C), and TA5 (8.488×10^{-6}/°C) in the range from RT to 600 °C. An increasing trend was observed with increasing Al_2O_3 substitution for each composition, with CTE values similar to that of bonded ceramics, ranging from approximately 7.4-8.4 $\times 10^{-6}$/°C.

Figure 15 shows images of the bonding interfaces after bonding the glass-ceramic to alumina substrates followed by heat treatment at 1000 and 1100°C, respectively. At 1000°C, no bonding was observed for TA0, TA1, and TA3; complete bonding between the substrate and glass-ceramic was observed only for TA5. At 1100°C, bonding was confirmed between the glass-ceramic and alumina substrates for all compositions. However, for TA0 and TA1, the upper and lower substrates were not completely bonded, and some crack layers were observed. In the case of TA3 and TA5, complete bonding was achieved between the upper and lower substrates.

Conclusions

In this study, we observed the structural changes and mechanical-property variations of a CASTZ-based glass-ceramic following Al_2O_3 substitution, and evaluated its potential utilization as a coating glass-ceramic in bonding applications. Through DTA, a second crystallization temperature (T_{P2}) was observed upon the substitution of Al_2O_3, and titanite was observed as the main crystal phase with willemite or anorthite as the secondary crystal phase, for all compositions. SEM and EDS revealed microstructural changes associated with the substitution level and heat-treatment temperature variations, accompanied by sharp changes in the hardness with increasing heat-treatment temperature. In particular, a trend of increasing hardness up to 8.97 GPa was observed for TA3 upon heat treatment at 1000°C, followed by a subsequent decrease. The titanite crystalline phase was confirmed through Raman spectroscopy and the highest hardness value was observed at TA3 owing to the increased Al_2O_3 substitution, indicating enhanced network stability. The bonding potential with alumina substrates was assessed using thermal expansion coefficients, which confirmed the strong bonding characteristics with alumina substrates. The CSTZ-Al_2O_3 glass-ceramic composition designed through this study was confirmed to be capable of changing the glass structure and increasing the hardness of crystallization, depending on the amount of substitution at a temperature of 1000°C. It exhibited a CTE similar to that of the base material; therefore, it is expected to be used as a glass-ceramic coating in bonding applications.

Declaration of Competing Interest

The authors declare that they have no known competing financial interests or personal relationships that could have appeared to influence the work reported in this paper.

Acknowledgments

This work was supported by Kyonggi University's Graduate Research Assistantship 2024.

References

1. M. Chen, M. Shen, X. Wang, S. Zhu, and F. Wang, Surf. Coat. Technol. 216 (2013) 145-151.
2. W. Zhu, L. Zhou, M. Tang, H. Zou, Y. Han, and X. Ran, J. Eur. Ceram. Soc. 41 (2021) 351-357.
3. D. Zheng, S. Zhu, and F. Wang, Surf. Coat. Technol. 200 (2006) 5931-5936.
4. L. Hallmann, P. Ulmer, and M. Kern, J. Mech. Behav. Biomed. Mater. 82 (2018) 355-370.
5. J. You, G. Jiang, and K. Xu, J. Non-Cryst. Solids. 282 (2001) 125-131.
6. J.H. Park, J. Non-Cryst. Solids. 358 (2012) 3096-3102.
7. Z. Xiao, J. Cheng, and H. Wu, J. Chin. Ceram. Soc. 40[7] (2012) 1000-1005.
8. M. Sajid, C. Bai, M. Aamir, Z. You, Z. Yan, and X. Lv, ISIJ Int. 59[7] (2019) 1153-1166.
9. M. Wang, J. Cheng, M. Li, and F. He, Phys. B (Amsterdam, Neth.) 406 (2011) 3865-3869.
10. A. Mehdilo, M. Irannajad, and B. Rezai, Miner. Eng. 70 (2015) 64-76.
11. T. Yamashita and P. Hayes, Appl. Surf. Sci. 254 (2008) 2441-2449.
12. B. Bharti, S. Kumar, H. Nolee, and R. Kumar, Sci. Rep. 6 (2016) 32355.
13. E. Kleebusch, C. Patzig, T. Höche, and C. Rüssel, Ceram. Int. 44 (2018) 2919-2926.
14. M. Chavoutier, D. Caurant, O. Majérus, R. Boulesteix, P. Loiseau, C. Jousseaume, E. Brunet, and E. Lecomte, J. Non-Cryst. Solids. 384 (2014) 15-24.
15. L.H.C. Andrade, S.M. Lima, A. Novatski, A.M. Neto, A.C. Bento, M.L. Baesso, F.C.G. Gandra, Y. Guyot, and G. Boulon, Phys. Rev. B. 78 (2008) 224202.
16. H. Masai, T. Ueno, T. Toda, Y. Takahashi, and T. Fujiwara, J. Non-Cryst. Solids. 356 (2010) 3080-3084.
17. K. Gasek, J. Partyka, M. Gajek, and W. Panna, J. Therm. Anal. Calorim. 125 (2016) 1135-1142.
18. P. Loiseau, D. Caurant, O. Majerus, N. Baffier, and C. Fillet, J. Mater. Sci. 38 (2003) 853-864.
19. A. Escardino, J.L. Amoro's, A. Gozalbo, M.J. Orts, and A. Moreno, J. Am. Ceram. Soc. 83[12] (2000) 2938-2944.
20. M. Rahimi, B. Sadeghi, and M.K. Razi, Int. J. Adv. Des. Manuf. Technol. 14[3] (2021) 25-33.
21. X. Jun, X. Zifan, Z. Weihong, L. Ye, and C. Jinshu, Key Eng. Mater. 509 (2012) 339-345.
22. D. Li, J.W. Guo, X.S. Wang, S.F. Zhang, and L. He, Mater. Sci. Eng. A. 669 (2016) 332-339.
23. Z. Zhang, J. Guo, Y. Sun, B. Tian, X. Zheng, M. Zhou, L. He, and S. Zhang, J. Mech. Behav. Biomed. Mater. 81 (2018) 52-60.
24. T. Fuss, A.M. Milankovic, C.S. Ray, C.E. Lesher, R.

Youngman, and D.E. Day, J. Non-Cryst. Solids. 352 (2006) 4101-4111.
25. E.A.P.D. Maeyer, R.M.H. Verbeeck, and C.W.J. Vercruysse, J. Dent. Res. 81. [8] (2002) 552-555.
26. M. Zhang, E.K.H. Salje, S.A.T. Redfern, U. Bismayer, and L.A. Groat, J. Phys.: Condens. Matter. 25 (2013) 115402.
27. B.O. Mysen, D. Virgo, and C.M. Scarfe, Am. Mineral. 65 (1980) 690-710.
28. W. Xua, Z. Cao, R. Ma, N. Wu, and S. Ouyang, J. Ceram. Process. Res. 24[3] (2023) 512-524.
29. J. You, G. Jiang, and K. Xu, J. Non-Cryst. Solids. 282 (2001) 125-131.
30. J. Liu, W. Kong, X. Yang, Q. Wang, Z. He, and X. Hou, Metals. 12[5] (2022) 715.
31. W. Xu, K. Shen, Z. Cao, F. Liu, Y. Zhang, T. Zhang, N. Wu, and S. Ouyang, Mater. Chem. Phys. 263 (2021) 124334.
32. G.W. Liu, G.J. Qiao, H.J. Wang, J.P. Wang, and T.J. Lu, J. Mater. Eng. Perform. 20 (2011) 1563-1568.
33. L. Esposito and A. Bellosi, J. Mater. Sci. 40 (2005) 2493-2498.
34. F. Smeacetto, M. Salvo, M. Ferraris, V. Casalegno, P. Asinari, and A. Chrysanthou, J. Eur. Ceram. Soc. 28 (2008) 2521-2527.